

Floquet higher-order topological insulator in a periodically driven bipartite lattice

Weiwei Zhu¹, Y. D. Chong,^{2,3,*} and Jiangbin Gong^{1,†}

¹Department of Physics, National University of Singapore, Singapore 117542, Singapore

²Division of Physics and Applied Physics, School of Physical and Mathematical Sciences,

Nanyang Technological University, Singapore 637371, Singapore

³Centre for Disruptive Photonic Technologies, Nanyang Technological University, Singapore 637371, Singapore



(Received 9 October 2020; accepted 17 December 2020; published 6 January 2021)

Floquet higher-order topological insulators (FHOTIs) are a novel topological phase that can occur in periodically driven lattices. An appropriate experimental platform to realize FHOTIs has not yet been identified. We introduce a periodically driven bipartite (two-band) system that hosts FHOTI phases without static counterparts, and predict that this lattice can be realized in experimentally realistic optical waveguide arrays, similar to those previously used to study anomalous Floquet insulators. The model exhibits interesting phase transitions from first-order to second-order topological matter by tuning a coupling strength parameter, without breaking lattice symmetry. In the FHOTI phase, the lattice hosts corner modes at eigenphase 0 or π , which are robust against disorder in the individual couplings.

DOI: [10.1103/PhysRevB.103.L041402](https://doi.org/10.1103/PhysRevB.103.L041402)

Introduction. Nonequilibrium topological matter generated by periodic driving has been a frontier research topic during the past decade [1]. Periodically driven or “Floquet” systems can realize exotic topological phases not found in static systems, such as Floquet π modes [2,3], anomalous Floquet insulators (AFIs) [4], and space-time symmetry protected topological insulators [5]. This has motivated theoretical and experimental studies of light-irradiated materials [6–10] as well as driven cold-atom systems [11]. Floquet topological phases can also be realized in time-independent platforms such as coupled optical resonators or oriented scattering networks [12–17] and optical waveguide arrays [18–24], in which the process of scattering or wave propagation simulates the time evolution of a wave function.

Higher-order topological insulators (HOTIs) are an intriguing group of topological phases [25,26] that feature gapped first-order boundary and gapless higher-order boundary. Soon after the discovery of HOTIs, several groups have investigated the possibility of realizing Floquet HOTIs (FHOTIs) [27–40], such as the use of driving schemes whose instantaneous Hamiltonians possess the symmetries of static HOTIs [28–30,32–34], as well as the use of peculiar space-time symmetries that are unique to periodically driven systems [31,35,36]. To date, it remains unclear what is the ideal experimental platform for realizing a FHOTI and studying its properties.

Here, we present a periodically driven bipartite square lattice model hosting FHOTI phases that should be easily experimentally accessible. Unlike previous FHOTI proposals that have required either negative hopping/coupling [33,34], or spin-orbital or superconducting interactions [28–32,35–40], our model involves a simple two-band single-particle

Hamiltonian with only periodic time modulation in the on-site potential differences and nearest-neighbor couplings, and with all couplings strictly non-negative throughout the driving protocol. These features allow the model to be implemented in experimental platforms such as optical waveguide arrays [18–24] and coupled optical resonator lattices [12–17] (i.e., minor variations of the experimental setups previously used to realize Floquet topological insulators [19–23]). Furthermore, because the system has only two bands, it becomes possible to excite the edge mode or corner mode by a single-site source, thus simplifying experimental procedures in probing and distinguishing between bulk, edge, and corner modes. The model proposed here thus offers a highly promising route to the experimental realization of FHOTI phases. These corner modes are unique to nonequilibrium systems without static counterparts, in the sense that they exist despite zero polarization and vanishing quadrupole moments.

Model. Consider a tight-binding model of a bipartite square lattice containing periodically modulated stepwise nearest-neighbor couplings. As shown in Fig. 1(a), the modulation consists of eight steps of equal duration $T/8$, where T is the modulation period. At odd steps, one of the four sets of nearest-neighbor couplings is activated (so an instantaneous system is dimerized). At even steps, the two sublattices A and B (red and blue) experience a potential difference. The time-dependent Bloch Hamiltonian thus becomes

$$H(\mathbf{k}, t) = \sum_{m=1,3,5,7} \theta_m(t) (e^{i\mathbf{b}_m \cdot \mathbf{k}} \sigma^+ + \text{H.c.}) + \Delta(t) \sigma_z, \quad (1)$$

where $\theta_m(t)$ is set to be θ during the m th (modulo 8) step, and zero at other time steps; $\Delta(t)$ equals Δ at even steps, and zero at odd steps; $\sigma^\pm = (\sigma_x \pm i\sigma_y)/2$, where $\sigma_{x,y,z}$ are Pauli matrices; and the vectors \mathbf{b}_{2n+1} are given by $-\mathbf{b}_1 = \mathbf{b}_5 = (0, a)$ and $-\mathbf{b}_3 = \mathbf{b}_7 = (a, 0)$, where a is the lattice constant. We always assume $T = 8$ and $a = 1$ and discuss all variables in dimensionless units.

*yidong@ntu.edu.sg

†phygj@nus.edu.sg

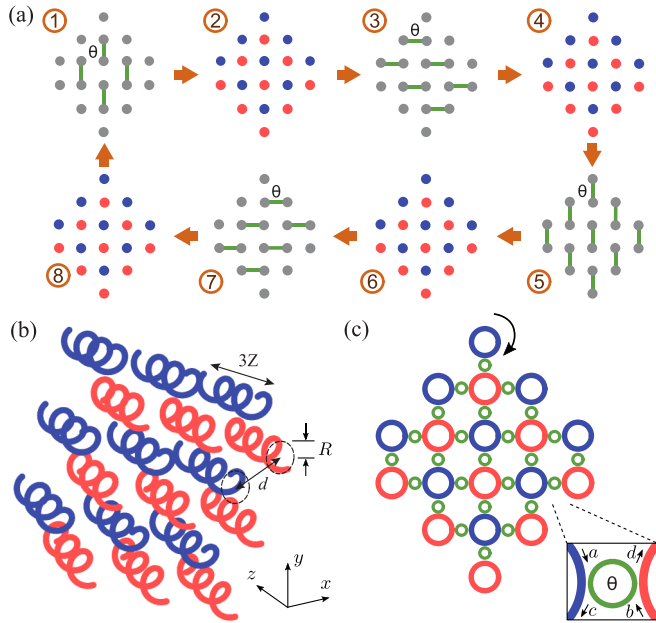


FIG. 1. Periodic modulation protocol for realizing a Floquet higher-order topological insulator (FHOTI). (a) Driving protocol for sites in a square lattice. During even time steps, the sites are decoupled and the two sublattices (red and blue circles) experience an energy bias $\pm\Delta$. During each odd time step, one of the four possible nearest-neighbor couplings is activated with hopping strength θ . (b) Waveguide array equivalent to (a) for a given choice of axial (z) propagation direction. The waveguides are helical, with neighboring waveguides staggered by a half period along z . (c) Lattice of coupled ring resonators, which is equivalent to (a) for a choice of light propagation direction within the rings. Nearest-neighbor site rings (red and blue circles) are coupled by off-resonant auxiliary coupling rings (green circles).

Using the instantaneous Hamiltonian, we define the Floquet operator (i.e., the time evolution operator over one period), $U_F \equiv \mathcal{T} \exp[-i \int_{t_0}^{t_0+T} H(\tau) d\tau]$, where \mathcal{T} is the time-ordering operator and t_0 is a reference time. We identify solutions $|\psi(t)\rangle = e^{-i\epsilon t} |\phi(t)\rangle$, with $|\phi(t)\rangle = |\phi(t+T)\rangle$ and

$$U_F |\phi(t_0)\rangle = e^{-i\epsilon T} |\phi(t_0)\rangle. \quad (2)$$

The quasienergy ϵ is an angular variable with period $2\pi/T$. Floquet states with $\epsilon = \pm\pi/T$ are called π modes in the literature because their eigenphase is π .

The model proposed above can be realized using an optical waveguide array, as depicted in Fig. 1(b), or a coupled optical ring resonator lattice, as shown in Fig. 1(c). For the waveguide array, the propagation of the paraxial light field envelope maps onto a time-dependent Schrödinger equation; the helical waveguides at the A and B sites are staggered along the axial direction, which reproduces the stepwise activation of the intersite couplings [18–24] and hence yields the time-dependent Hamiltonian (1). In the coupled-ring platform, fixed-frequency light waves propagate within a lattice of “site rings” with a given circulation direction (i.e., either clockwise or anticlockwise within each ring, with no back-propagation); by accounting for the unitary scattering relations between the coupled rings, one can derive a spectral-band problem equivalent to the Floquet band eigenproblem of Eq. (2) [13,16].

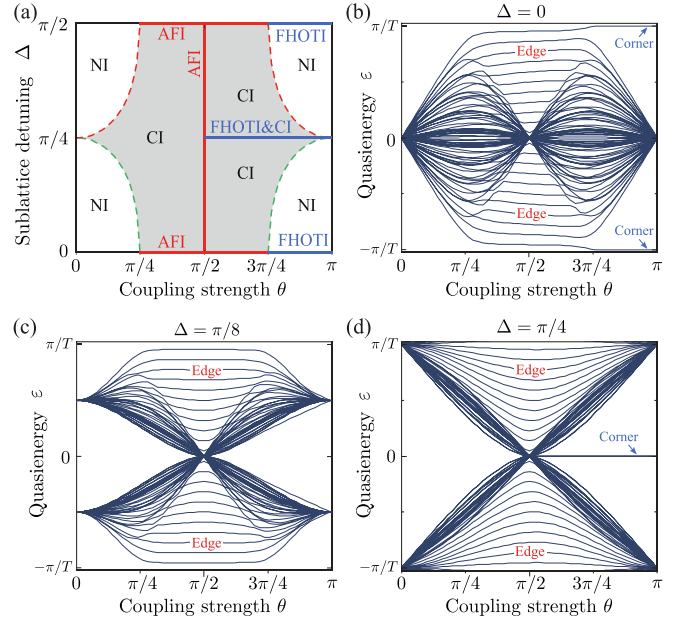


FIG. 2. (a) Phase diagram of the lattice vs coupling strength θ and Δ . Green (red) dashed lines are the phase transition point at the Γ (X) point. (b)–(d) Spectrum vs θ for a finite structure with eight unit cells along each edge direction. (b) For $\Delta = 0$, (c) for $\Delta = \pi/8$, and (d) for $\Delta = \pi/4$.

Topological phases. Figure 2(a) shows the obtained topological phase diagram, plotted against the potential bias parameter Δ and the coupling strength parameter θ . A quick inspection of Fig. 2(a) shows that several distinct topological phases are induced by periodic time modulation: normal insulator (NI), Floquet Chern insulator (CI), AFI [4], and FHOTI. At the phase boundaries, the band-crossing points occur at either the Γ or X points in the Brillouin zone, respectively indicated by green and red dashes in Fig. 2(a). The band crossings occur at these points because the Hamiltonian (1) is invariant under rotation by 90° (C_4) and a quarter-period translation in time: $H(\mathbf{k}, t) = H(C_4^{-1}\mathbf{k}, t + T/4)$, so that $U_F(\mathbf{k}) = U_F(C_4^{-1}\mathbf{k})$. The AFI phases (in which the Floquet band structure has a single nontrivial band gap) exist only along the red lines in Fig. 2(a). By contrast, the FHOTIs exist only along the shown blue lines, requiring $\Delta = 0$ (same as $\Delta = \pi/2$) or $\Delta = \pi/4$. The found FHOTI phases are protected by a combination of particle-hole symmetry and inversion symmetry, as explained below.

The band diagram for $\Delta = 0$ is shown in Fig. 2(b). In this case, there is a single bulk band, and the range of ϵ outside the band constitutes a single “band gap” (recall that ϵ is a periodic variable). For $0 \leq \theta < \pi/4$, the gap is topologically trivial; this is the NI phase. For $\pi/4 < \theta < 3\pi/4$, the gap is topologically nontrivial and spanned by edge modes; this is the AFI phase [4,12,13,16]. For $3\pi/4 < \theta < \pi$, the system is in the FHOTI phase with corner modes at $\epsilon = \pi/T$ ($-\pi/T$).

To intuitively understand the emergence of Floquet corner modes, it is useful to use the coupled ring lattice representation [13,16]. The stepwise intersite couplings in the Floquet system of Fig. 1(a) are equivalent to a set of unitary scattering relations. As shown in Fig. 1(c), these relations have the form

$[c, d]^T = \exp(-i\theta\sigma_x)[a, b]^T$, where $\{a, b, c, d\}$ are complex wave amplitudes in the incoming and outgoing arms of adjacent rings. For $\theta = \pi$, the scattering relation reduces to $-a \rightarrow c$ and $-b \rightarrow d$; the rings effectively become decoupled, with the inter-ring connection only contributing a π phase shift with each ring. Under these circumstances, one round of propagation within a bulk ring (which has four neighbors) or edge ring (which has two neighbors) acquires an even number of π phase shifts; however, one round around a corner ring (which has one neighbor) brings a π phase shift. This implies that there exist Floquet eigenstates with $\varepsilon T = 0$ localized to each bulk and edge site, but a separate set of Floquet eigenstates with $\varepsilon T = \pi$ localized to each corner site. For $\theta < \pi$, the corner modes persist so long as the gap remains open.

Figure 2(c) shows the band diagram for $\Delta = \pi/8$. Here, the system supports NI, AFI, and CI phases. The AFI phase exists only at $\theta = \pi/2$, when both bulk bands collapse to $\varepsilon = 0$. Figure 2(d) shows the band diagram for $\Delta = \pi/4$. This is the other scenario in which corner modes appear. For $0 < \theta < \pi/2$, the system is in an CI phase with two bulk bands, a trivial gap, and a nontrivial gap spanned by edge modes. For $\pi/2 < \theta \leq \pi$, the system features the coexistence of FHOTI and CI phases. There are two bulk bands, a gap spanned by edge modes, and a gap containing a corner mode pinned at $\varepsilon = 0$.

Symmetry analysis and robustness of FHOTIs. The corner modes are seen to only appear at $\Delta = n\pi/4$ where $n \in \mathbb{Z}$. This observation deserves a symmetry-based explanation. Interestingly, for $\Delta = n\pi/4$ the lattice possesses additional symmetries that protect such FHOTI phases. That is, without such underlying symmetries, the corner modes are unprotected and the system can be perturbed into the NI phase without closing the bulk gap, as indicated by the phase diagram [Fig. 2(a)].

Specifically, for $\Delta = 0$ (or, equivalently, any even multiple of $\pi/4$), the lattice obeys a particle-hole symmetry $CH(k, t)C = -H^*(-k, t)$ and inversion symmetry $\mathcal{I}H(k, t)\mathcal{I} = H(-k, t)$, where $C = \sigma_z$ and $\mathcal{I} = \sigma_x$. As such, in terms of the evolution operator, $CU_F(k_x, k_y)C = U_F^*(-k_x, -k_y)$ and $\mathcal{I}U_F(k_x, k_y)\mathcal{I} = U_F(-k_x, -k_y)$. For $\Delta = \pi/4$ and other odd multiples of $\pi/4$, the evolution operator satisfies $CU_F(k_x, k_y)C = U_F^*(\pi/a - k_x, -k_y)$ and $\mathcal{I}U_F(k_x, k_y)\mathcal{I} = U_F(\pi/a - k_x, -k_y)$. With either set of symmetries, the lattice belongs to the D class, which is associated with a \mathbb{Z}_2 topological invariant [41]. These FHOTI phases are thus adequately described by the existing classification scheme for static HOTIs.

The particle-hole symmetry guarantees that the corner modes come in pairs with quasienergy 0 or π/T , and the inversion symmetry further ensures that the paired corner modes are localized at different edges. So a single pair of corner modes cannot annihilate without bulk band closure. To verify this, we study lattices with disorder in the coupling strength that preserves the particle-hole and inversion symmetries. This is accomplished by setting $\theta = \theta_0(1 + D)$, with D randomly distributed in the range $-W < D < W$. As shown in Figs. 3(a) and 3(b) for $\theta_0 = 0.9\pi$, both the π corner mode (for $\Delta = 0$) and the 0 corner mode (for $\Delta = \pi/4$) are robust against the introduced disorder. With increasing W ,

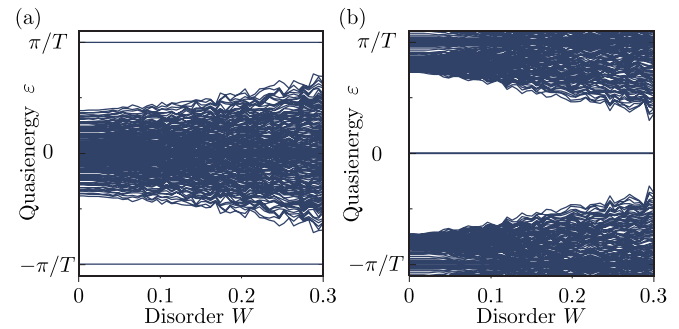


FIG. 3. Quasienergy spectra vs strength W of disorder introduced to the θ parameter. The finite lattices are of the same shape as in Fig. 1 but with eight unit cells along each direction. (a) $\Delta = 0$ and (b) $\Delta = \pi/4$.

the bulk band broadens but the corner modes remain intact, with their quasienergies unaltered. In the Supplemental Material [42], we show that if some disorder (weak compared with the band gap) is introduced to Δ , the in-gap corner modes are shifted from 0 or π but still survive. This indicates that even Δ need not be very precisely tuned in experiments. In addition, we investigate the role of time-dependent disorder, showing that $2T$ perturbations give rise to an interesting interplay between corner modes and chiral edge modes.

Experimental proposal for FHOTIs in waveguide arrays. Optical waveguide arrays are an appealing platform for exploring Floquet topological phases. Thus far, they have been used to realize Floquet Chern insulators and AFIs [18–24]. Here, we present continuum simulations (not limited to the tight-band approximation) showing that the above FHOTI model can be realized in experimentally realistic waveguide arrays. By decreasing the distance between neighboring waveguides, one can achieve topological phase transitions from NI to AFI, and subsequently to the FHOTI phase.

The evolution of light in a waveguide system is governed by the Schrödinger-like equation [43,44]

$$i\partial_z\psi = -\frac{1}{2k_0}\nabla_{\perp}^2\psi - \frac{k_0\delta n(x, y, z)}{n_0}\psi, \quad (3)$$

where x, y are the transverse directions, z is the axial direction, $\nabla_{\perp}^2 = \partial_x^2 + \partial_y^2$, n_0 is the background refractive index, $k_0 = 2\pi n_0/\lambda$, λ is the operating wavelength in free space, and $\delta n(x, y, z)$ is the modulation in the refractive index [18,19,24]. The axial coordinate z acts as a synthetic time coordinate. We take $n_0 = 1.473$ and $\lambda = 1550$ nm. The modulation function induces a bipartite square lattice with the unit cell configuration shown in Fig. 1(c), with both waveguides having clockwise helicity with helix radius $R = 4 \mu\text{m}$, period $Z = 2 \text{ cm}$, and mean waveguide separation d . Each waveguide has $\delta n = 2.6 \times 10^{-3}$, with an elliptical cross section with major and minor axes of 9.8 and 6.4 μm . All those parameters have been used in a previous experiment [45].

The band structure of the waveguide array is numerically obtained by extracting the fundamental modes of the waveguide, as described in Ref. [19]. We consider an array with zero detuning between the two sublattices (i.e., $\Delta = 0$). For this case, the phase transition is predicted to occur at the Γ point. Figure 4(a) shows the calculated bulk band

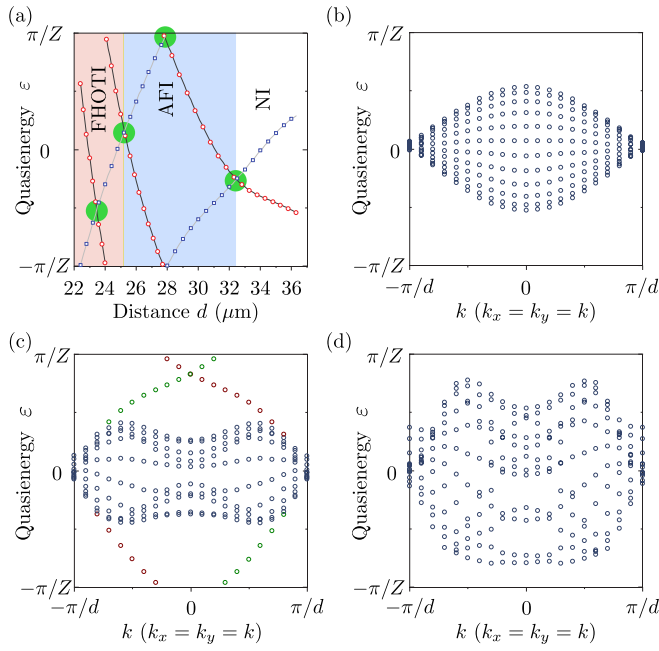


FIG. 4. Band diagrams for waveguide arrays with $\Delta = 0$. (a) Quasienergies at Γ (the center of the Brillouin zone) versus d . The band-crossing points, marked by green circles, appear to correspond (in order of decreasing d) to the tight-binding model's critical coupling strengths $\theta \in \{\pi/4, \pi/2, 3\pi/4, \pi\}$, respectively [see Fig. 2(a)]. (b)–(d) Band structures for a semi-infinite strip periodic along the (e_x, e_y) direction and six unit cells wide along the $(e_x, -e_y)$ direction, for (b) $d = 36 \mu\text{m}$, (c) $d = 28 \mu\text{m}$, and (d) $d = 23 \mu\text{m}$.

quasienergies at Γ , as a function of the waveguide separation d . For $d \rightarrow \infty$, the lattice must be in the NI phase ($\theta \rightarrow 0$). With decreasing d , we observe a band crossing at $d \approx 32.4 \mu\text{m}$, which should correspond to the NI-to-AFI transition at $\theta = \pi/4$ [Fig. 2(a)]. The third band crossing occurs at $d \approx 25.2 \mu\text{m}$ and should correspond to the AFI-to-FHOTI transition at $\theta = 3\pi/4$.

To verify the nature of these phases, Figs. 4(b)–4(d) show the Floquet band structures for $d = 36 \mu\text{m}$ (NI), $d = 28 \mu\text{m}$ (AFI), and $d = 23 \mu\text{m}$ (FHOTI), in a semi-infinite strip geometry. As expected, topological edge modes are observed in the AFI case [Fig. 4(c)]. The corner modes of the FHOTI phase cannot be seen here [Fig. 4(d)], since the strip geometry lacks corners.

Figure 5 shows simulation results for a finite waveguide array, computed using the split-step Fourier method [19]. At $z = 0$ (which corresponds to the maximal distance between the waveguides in the unit cell), a corner waveguide is excited. The intensities are plotted at different final values of z . For the NI, the initial corner excitation diffracts into the bulk [Fig. 5(a)]. For the AFI, the corner excitation couples to chiral edge modes that propagate around a corner [Fig. 5(b)]. For the FHOTI, the excitation remains localized, oscillating periodically between the few sites nearest to the corner. In Figs. 5(c) and 5(d), we plot the results at $6Z$ and $6.5Z$, for which the excitation is mostly confined to a single site (on the A sublattice at $6Z$ and the B sublattice at $6.5Z$). This interesting oscillation reflects the expected nontrivial micro-

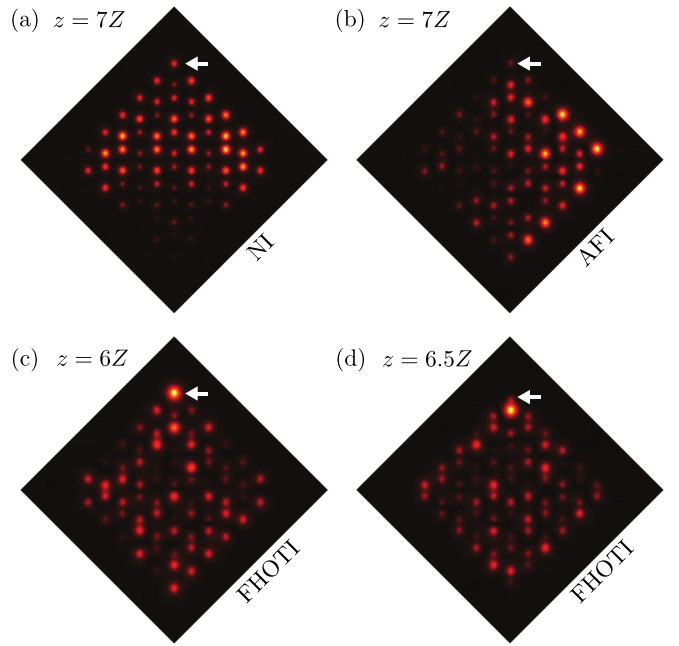


FIG. 5. Field intensity distributions in the optical waveguide array for different topological phases and propagation distances. (a) $d = 36 \mu\text{m}$ (NI phase) after $7Z$. (b) $d = 28 \mu\text{m}$ (AFI phase) after $7Z$. (c),(d) $d = 23 \mu\text{m}$ (FHOTI phase) after (c) $6Z$ and (d) $6.5Z$. The initially excited corner waveguide is indicated by a white arrow.

scopic dynamics of an edge mode at quasienergy π/T [3,46–48], but the observation here is even more interesting because it is due to a corner π mode. Note that we have only used single-site excitation to observe the differences between NI, AFI, and FHOTI; clearer signatures of edge or corner state localization may be obtainable by considering other initial states. In the Supplemental Material [42], we introduce a more complicated driving protocol that yields simultaneous 0 and π corner modes, which is of interest to studies of time crystals [49] and quantum information applications [38].

Conclusion and discussion. The engineering of a FHOTI phase typically started from a Floquet topological insulator with gapless edge modes, followed by breaking a symmetry to open a gap in the edge modes. By contrast, our model exhibits topological transitions between normal insulator, anomalous Floquet topological insulator, and FHOTI phases while preserving lattice symmetry. The used bipartite lattice, with strictly non-negative nearest-neighbor couplings, appears to be the simplest setup known to date for realizing a FHOTI. Variants of the model, based on honeycomb and triangular lattices rather than square lattices, can also realize FHOTI phases [42]. Continuum simulations show that our proposal can be realized in optical waveguide arrays of the sort that have previously been used to realize Floquet topological insulators experimentally. This work provides opportunities for studying the properties of these unusual topological phases, such as the interactions between corner modes and chiral edge modes.

Acknowledgments. We acknowledge funding support by the Singapore Ministry of Education Academic Research Fund Tier-3 (Grant No. MOE2017-T3-1-001 and WBS No.

R-144-000-425-592) and by the Singapore NRF Grant No. NRF-NRFI2017-04 (WBS No. R-144-000-378- 281). We are

grateful to L. Li, M. Umer, R. Bomantara, H. Xue, and B. Zhang for helpful discussions.

-
- [1] M. S. Rudner and N. H. Lindner, Band structure engineering and non-equilibrium dynamics in Floquet topological insulators, *Nat. Rev. Phys.* **2**, 229 (2020).
- [2] L. Jiang, T. Kitagawa, J. Alicea, A. R. Akhmerov, D. Pekker, G. Refael, J. I. Cirac, E. Demler, M. D. Lukin, and P. Zoller, Majorana Fermions in Equilibrium and in Driven Cold-Atom Quantum Wires, *Phys. Rev. Lett.* **106**, 220402 (2011).
- [3] Q.-J. Tong, J.-H. An, J. B. Gong, H.-G. Luo, and C. H. Oh, Generating many Majorana modes via periodic driving: A superconductor model, *Phys. Rev. B* **87**, 201109(R) (2013).
- [4] M. S. Rudner, N. H. Lindner, E. Berg, and M. Levin, Anomalous Edge States and the Bulk-Edge Correspondence for Periodically Driven Two-Dimensional Systems, *Phys. Rev. X* **3**, 031005 (2013).
- [5] T. Morimoto, H. C. Po, and A. Vishwanath, Floquet topological phases protected by time glide symmetry, *Phys. Rev. B* **95**, 195155 (2017).
- [6] T. Oka and H. Aoki, Photovoltaic Hall effect in graphene, *Phys. Rev. B* **79**, 081406(R) (2009).
- [7] T. Kitagawa, E. Berg, M. Rudner, and E. Demler, Topological characterization of periodically driven quantum systems, *Phys. Rev. B* **82**, 235114 (2010).
- [8] T. Kitagawa, T. Oka, A. Brataas, L. Fu, and E. Demler, Transport properties of nonequilibrium systems under the application of light: Photoinduced quantum Hall insulators without Landau levels, *Phys. Rev. B* **84**, 235108 (2011).
- [9] J. W. McIver, B. Schulte, F. U. Stein, T. Matsuyama, G. Jotzu, G. Meier, and A. Cavalleri, Light-induced anomalous Hall effect in graphene, *Nat. Phys.* **16**, 38 (2020).
- [10] H. Hübener, M. A. Sentef, U. D. Giovannini, A. F. Kemper, and A. Rubio, Creating stable Floquet-Weyl semimetals by laser-driving of 3D Dirac materials, *Nat. Commun.* **8**, 13940 (2017).
- [11] K. Wintersperger, C. Braun, F. N. Ünal, A. Eckardt, M. D. Liberto, N. Goldman, I. Bloch, and M. Aidelsburger, Realization of an anomalous Floquet topological system with ultracold atoms, *Nat. Phys.* **16**, 1058 (2020).
- [12] G. Q. Liang and Y. D. Chong, Optical Resonator Analog of a Two-Dimensional Topological Insulator, *Phys. Rev. Lett.* **110**, 203904 (2013).
- [13] M. Pasek and Y. D. Chong, Network models of photonic Floquet topological insulators, *Phys. Rev. B* **89**, 075113 (2014).
- [14] W. C. Hu, J. C. Pillay, K. Wu, M. Pasek, P. P. Shum, and Y. D. Chong, Measurement of a Topological Edge Invariant in a Microwave Network, *Phys. Rev. X* **5**, 011012 (2015).
- [15] F. Gao, Z. Gao, X. H. Shi, Z. J. Yang, X. Lin, H. Y. Xu, J. D. Joannopoulos, M. Soljačić, H. S. Chen, L. Lu, Y. D. Chong, and B. L. Zhang, Probing topological protection using a designer surface plasmon structure, *Nat. Commun.* **7**, 11619 (2016).
- [16] P. Delplace, M. Fruchart, and C. Tauber, Phase rotation symmetry and the topology of oriented scattering networks, *Phys. Rev. B* **95**, 205413 (2017).
- [17] S. Afzal, T. J. Zimmerling, Y. Ren, D. Perron, and V. Van, Realization of Anomalous Floquet Insulators in Strongly Coupled Nanophotonic Lattices, *Phys. Rev. Lett.* **124**, 253601 (2020).
- [18] M. C. Rechtsman, J. M. Zeuner, Y. Plotnik, Y. Lumer, D. Podolsky, F. Dreisow, S. Nolte, M. Segev, and A. Szameit, Photonic Floquet topological insulators, *Nature (London)* **496**, 196 (2013).
- [19] D. Leykam, M. C. Rechtsman, and Y. D. Chong, Anomalous Topological Phases and Unpaired Dirac Cones in Photonic Floquet Topological Insulators, *Phys. Rev. Lett.* **117**, 013902 (2016).
- [20] L. J. Maczewsky, J. M. Zeuner, S. Nolte, and A. Szameit, Observation of photonic anomalous Floquet topological insulators, *Nat. Commun.* **8**, 13756 (2017).
- [21] S. Mukherjee, A. Spracklen, M. Valiente, E. Andersson, P. Öhberg, N. Goldman, and R. R. Thomson, Experimental observation of anomalous topological edge modes in a slowly driven photonic lattice, *Nat. Commun.* **8**, 13918 (2017).
- [22] S. Mukherjee, H. K. Chandrasekharan, P. Öhberg, N. Goldman, and R. R. Thomson, State-recycling and time-resolved imaging in topological photonic lattices, *Nat. Commun.* **9**, 4209 (2018).
- [23] L. J. Maczewsky, B. Höckendorf, M. Kremer, T. Biesenthal, M. Heinrich, A. Alvermann, H. Fehske, and A. Szameit, Fermionic time-reversal symmetry in a photonic topological insulator, *Nat. Mater.* **19**, 855 (2020).
- [24] S. Mukherjee and M. C. Rechtsman, Observation of Floquet solitons in a topological bandgap, *Science* **368**, 856 (2020).
- [25] W. A. Benalcazar, B. A. Bernevig, and T. L. Hughes, Quantized electric multipole insulators, *Science* **357**, 61 (2017).
- [26] F. Schindler, A. M. Cook, M. G. Vergniory, Z. J. Wang, S. S. P. Parkin, B. A. Bernevig, and T. Neupert, Higher-order topological insulators, *Sci. Adv.* **4**, eaat0346 (2018).
- [27] R. W. Bomantara, L. W. Zhou, J. X. Pan, and J. B. Gong, Coupled-wire construction of static and Floquet second-order topological insulators, *Phys. Rev. B* **99**, 045441 (2019).
- [28] M. Rodriguez-Vega, A. Kumar, and B. Seradjeh, Higher-order Floquet topological phases with corner and bulk bound states, *Phys. Rev. B* **100**, 085138 (2019).
- [29] R. Seshadri, A. Dutta, and D. Sen, Generating a second-order topological insulator with multiple corner states by periodically driving, *Phys. Rev. B* **100**, 115403 (2019).
- [30] T. Nag, V. Juricic, and B. Roy, Out of equilibrium higher-order topological insulator: Floquet engineering and quench dynamics, *Phys. Rev. Research* **1**, 032045R (2019).
- [31] Y. Peng and G. Refael, Floquet Second-Order Topological Insulators from Nonsymmorphic Space-Time Symmetries, *Phys. Rev. Lett.* **123**, 016806 (2019).
- [32] A. K. Ghosh, G. C. Paul, and A. Saha, Higher order topological insulator via periodic driving, *Phys. Rev. B* **101**, 235403 (2020).
- [33] H. P. Hu, B. Huang, E. H. Zhao, and W. V. Liu, Dynamical Singularities of Floquet Higher-Order Topological Insulators, *Phys. Rev. Lett.* **124**, 057001 (2020).

- [34] B. Huang and W. V. Liu, Floquet Higher-Order Topological Insulators with Anomalous Dynamical Polarization, *Phys. Rev. Lett.* **124**, 216601 (2020).
- [35] Y. Peng, Floquet higher-order topological insulators and superconductors with space-time symmetries, *Phys. Rev. Research* **2**, 013124 (2020).
- [36] S. Chaudhary, A. Haim, Y. Peng, and G. Refael, Phonon-induced Floquet second-order topological phases protected by space-time symmetries, [arXiv:1911.07892](https://arxiv.org/abs/1911.07892).
- [37] R. W. Bomantara, Time-Induced Second-Order Topological Superconductors, *Phys. Rev. Research* **2**, 33495 (2020).
- [38] R. W. Bomantara and J. B. Gong, Measurement-only quantum computation with Floquet Majorana corner modes, *Phys. Rev. B* **101**, 085401 (2020).
- [39] A. K. Ghosh, T. Nag, and A. Saha, Floquet generation of second order topological superconductor, [arXiv:2009.11220](https://arxiv.org/abs/2009.11220).
- [40] R. X. Zhang and Z. C. Yang, Tunable fragile topology in Floquet systems, [arXiv:2005.08970](https://arxiv.org/abs/2005.08970).
- [41] E. Khalaf, Higher-order topological insulators and superconductors protected by inversion symmetry, *Phys. Rev. B* **97**, 205136 (2018).
- [42] See Supplemental Material at <http://link.aps.org/supplemental/10.1103/PhysRevB.103.L041402> for details on realizing Floquet π and 0 corner modes with a different driving protocol applied to a two-band square lattice system, more disorder effects, as well as how our proposal can be applied to honeycomb lattice and triangular lattice systems.
- [43] D. N. Christodoulides, F. Lederer, and Y. Silberberg, Discretizing light behavior in linear and nonlinear waveguide lattices, *Nature (London)* **424**, 817 (2003).
- [44] I. L. Garanovich, S. Longhi, A. A. Sukhorukov, and Y. S. Kivshar, Light propagation and localization in modulated photonic lattices and waveguides, *Phys. Rep.* **518**, 1 (2012).
- [45] J. Noh, S. Huang, D. Leykam, Y. D. Chong, K. P. Chen, and M. C. Rechtsman, Experimental observation of optical Weyl points and Fermi arc-like surface states, *Nat. Phys.* **13**, 611 (2017).
- [46] J. K. Asbóth and H. Obuse, Bulk-boundary correspondence for chiral symmetric quantum walks, *Phys. Rev. B* **88**, 121406(R) (2013).
- [47] J. K. Asbóth, B. Tarasinski, and P. Delplace, Chiral symmetry and bulk-boundary correspondence in periodically driven one-dimensional systems, *Phys. Rev. B* **90**, 125143 (2014).
- [48] Q. Q. Cheng, Y. M. Pan, H. Q. Wang, C. S. Zhang, D. Yu, A. Gover, H. J. Zhang, T. Li, L. Zhou, and S. N. Zhu, Observation of Anomalous π Modes in Photonic Floquet Engineering, *Phys. Rev. Lett.* **122**, 173901 (2019).
- [49] R. W. Bomantara and J. B. Gong, Simulation of Non-Abelian Braiding in Majorana Time Crystals, *Phys. Rev. Lett.* **120**, 230405 (2018).